Supplementary Information (SI) for Inorganic Chemistry Frontiers.
This journal is © the Partner Organisations 2026

Supporting Information

3D-printed binder-free $Na_3V_2(PO_4)_3$ 3D cathode with adjustable porosity for sodium-ion batteries

Jingyu Chen, Pengfei Bi, Yingyue Tan, Jilong Ma, Xin Liu, Huijuan Zhang, Jinling Ma*, Yu Wang*

Jingyu Chen, Pengfei Bi, Jinling Ma, Yingyue Tan, Jilong Ma, Xin. Liu,
State Key Laboratory of Power Transmission Equipment Technology, School of Electrical Engineering, Chongqing University, 174 Shazheng Street, Shapingba District, Chongqing City, 400044, P.R. China
E-mail: mjl201909@cqu.edu.cn

Huijuan Zhang, Yu Wang
State Key Laboratory of Power Transmission Equipment Technology, School of Chemistry and Chemical Engineering, Chongqing University, 174 Shazheng Street, Shapingba District, Chongqing City, 400044, PR China
E-mail: wangy@cqu.edu.cn

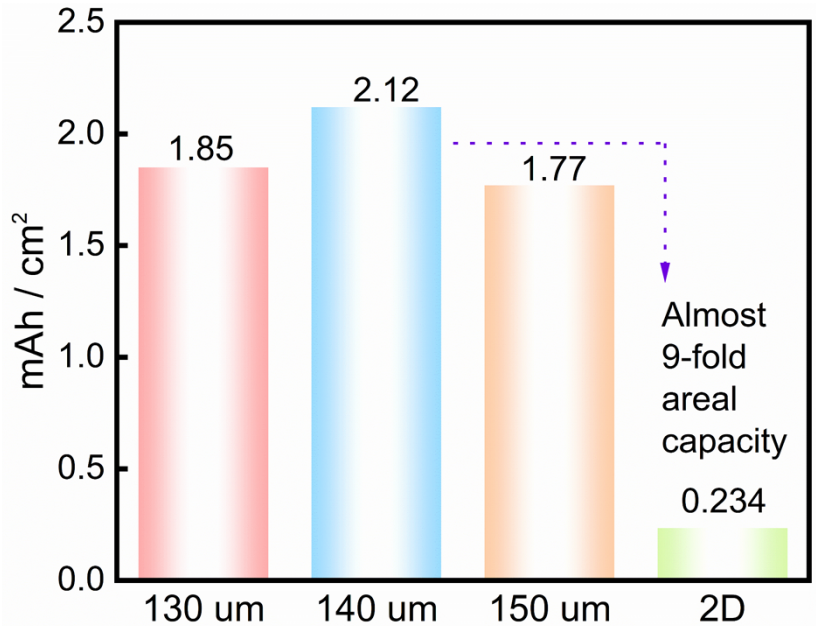

Fig. S1 The areal capacity between 3D NVP electrode in this work and conventional 2D NVP electrode.

In the laboratory-based research on sodium vanadium phosphate (NVP) cathode material in sodium-ion batteries, the commonly used standard experimental protocol typically sets the electrode loading within the range of 1.0 - 2.0 mg·cm^{-2}.[1] Based on the theoretical specific capacity of NVP of 117 mAh·g^{-1} and the assumed conventional 2D NVP electrode maximum load of 2 mg·cm^{-2}, the areal capacity of the conventional 2D NVP electrode is estimated to be 0.234 mAh·cm^{-2}. By comparison, the diameter of 140 μm beams 3D NVP electrode in this work exhibits an areal capacity of 2.12 mAh·cm^{-2} (Fig. S1), which is approximately 9 times higher than that of its conventional 2D NVP electrode (0.234 mAh·cm^{-2}), demonstrating the areal capacity advantage of the 3D NVP electrode compared to conventional 2D NVP electrode.

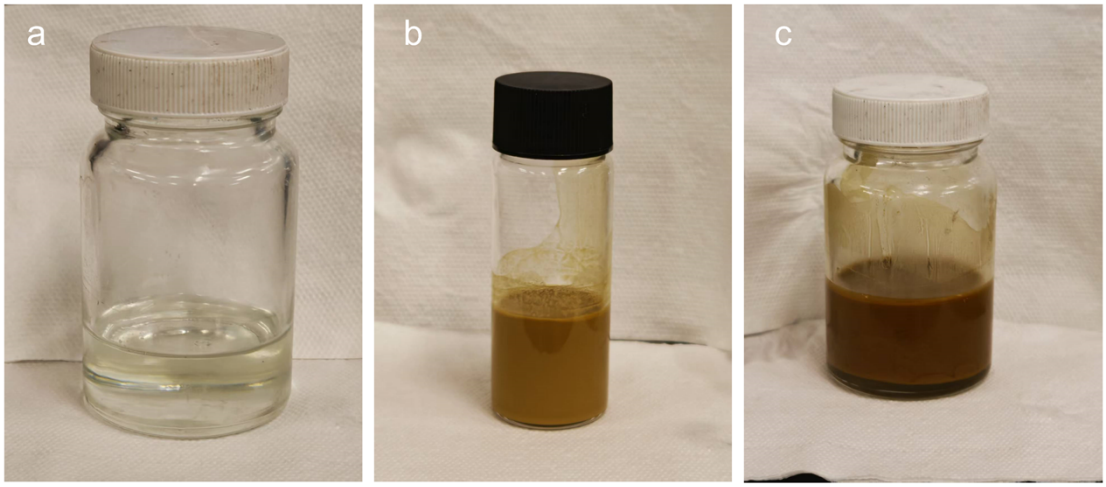

Fig. S2 Optical images of (a) commercial resin, (b) NVP precursor solution, (c) the printing ink.

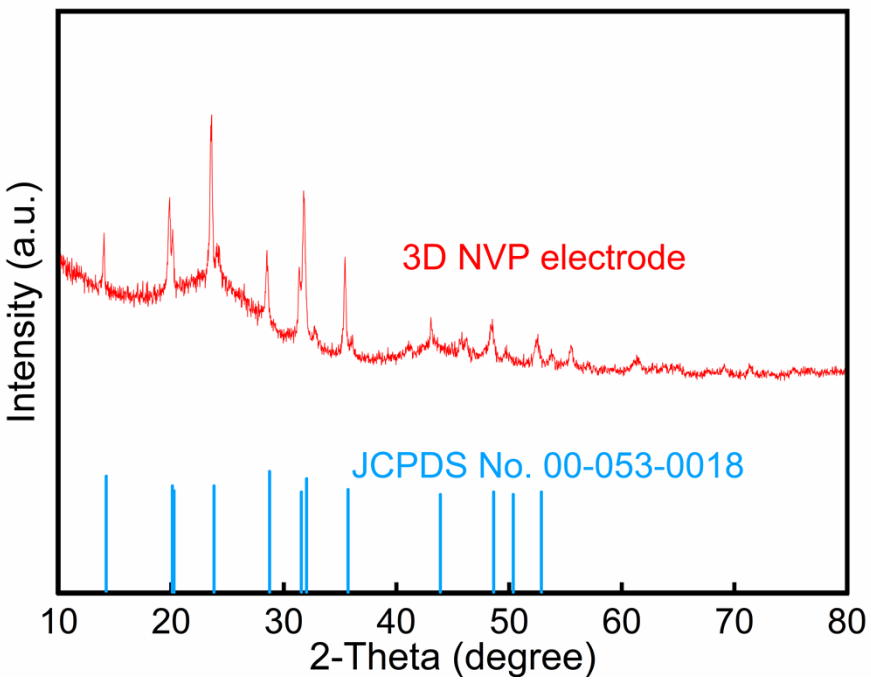

Fig. S3 XRD patterns of 3D NVP electrode.

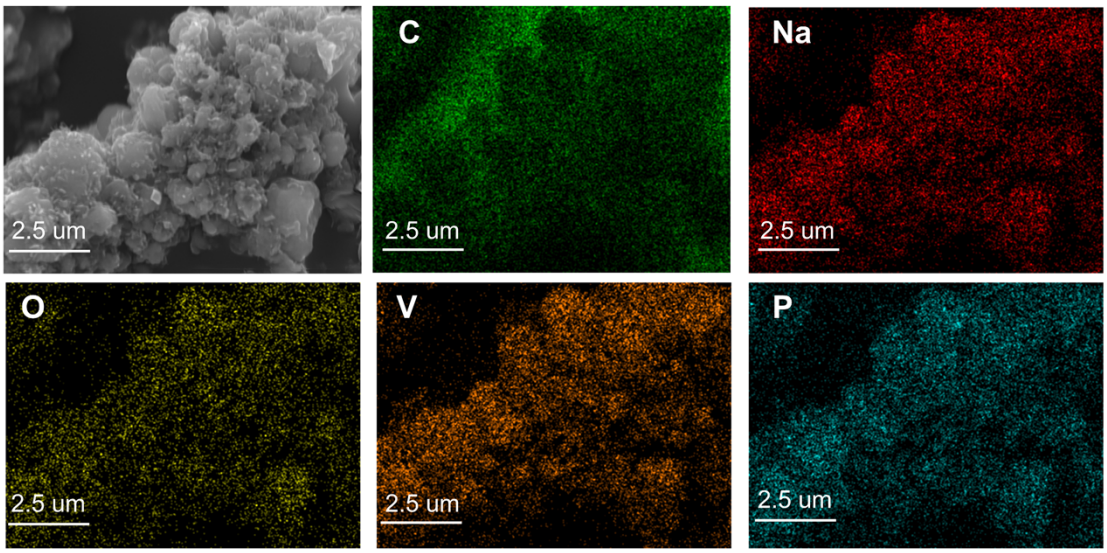

Fig. S4 Energy-dispersive spectroscopy mapping for 3D NVP electrode.

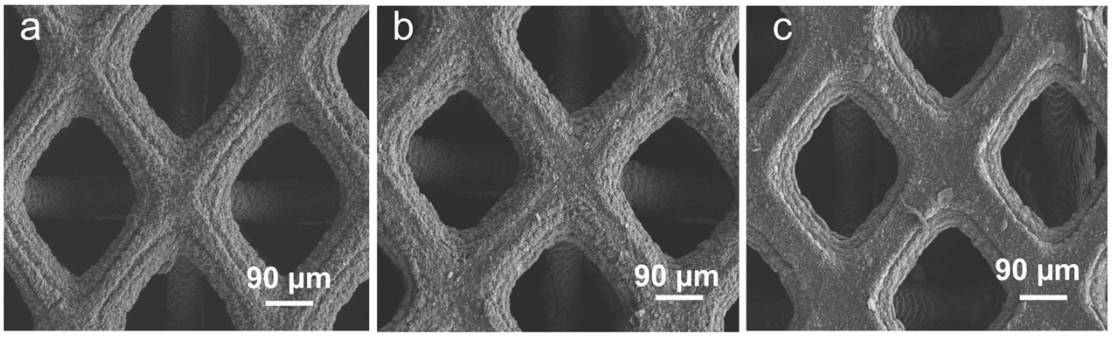

Fig. S5 SEM images with low magnification resolution showing the porosity under beam thicknesses of (a) 130 µm, (b) 140 µm, (c) and 150 µm.

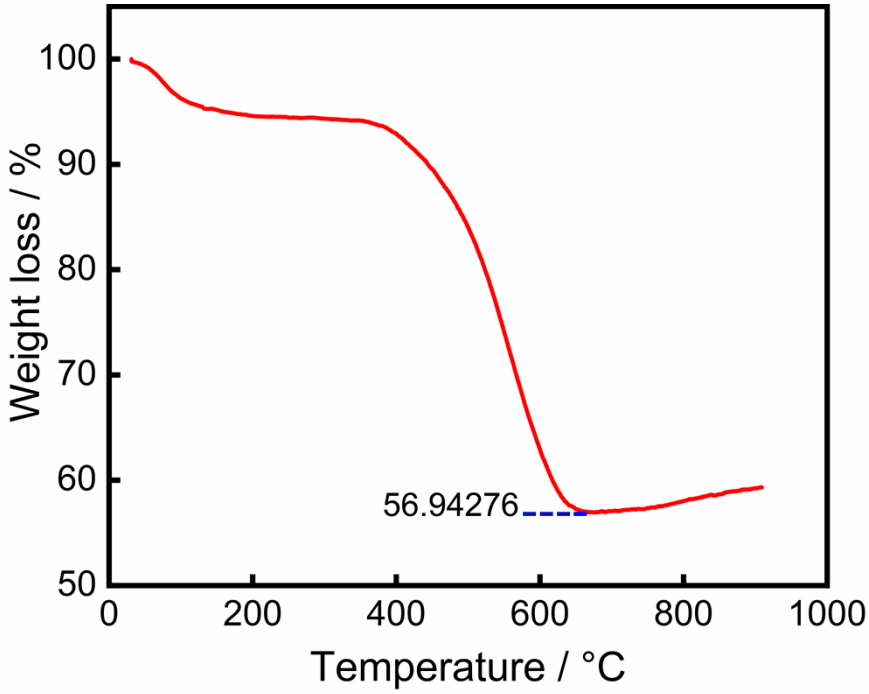

Fig. S6 TGA curve of 3D NVP electrode.

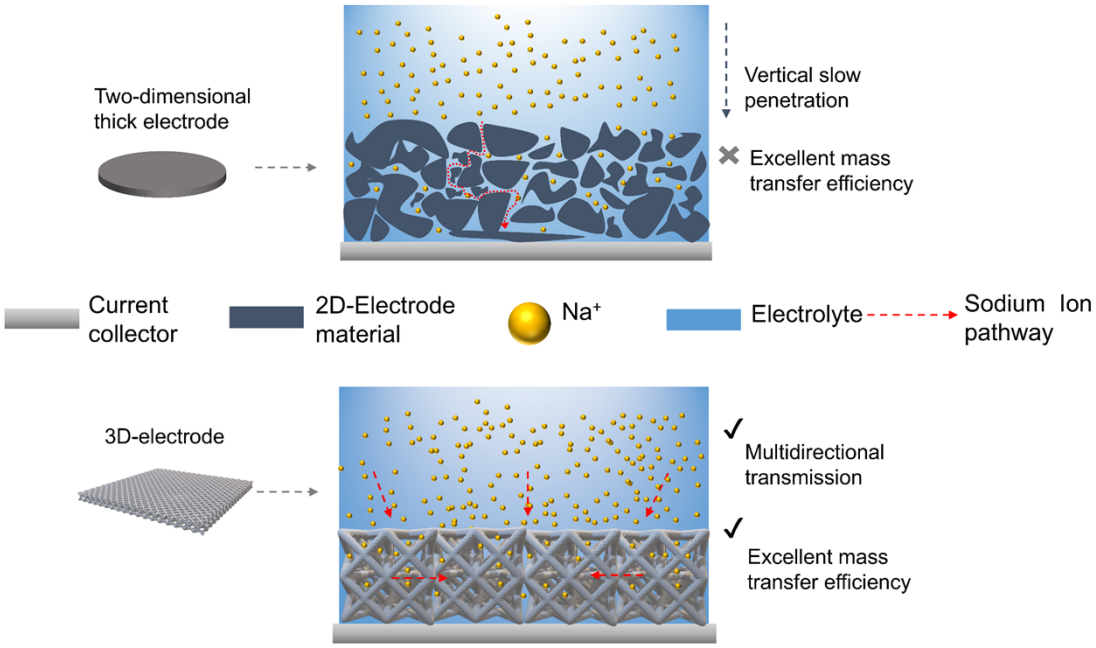

Fig. S7 Schematic diagram of ion transport in 2D and 3D NVP electrodes.

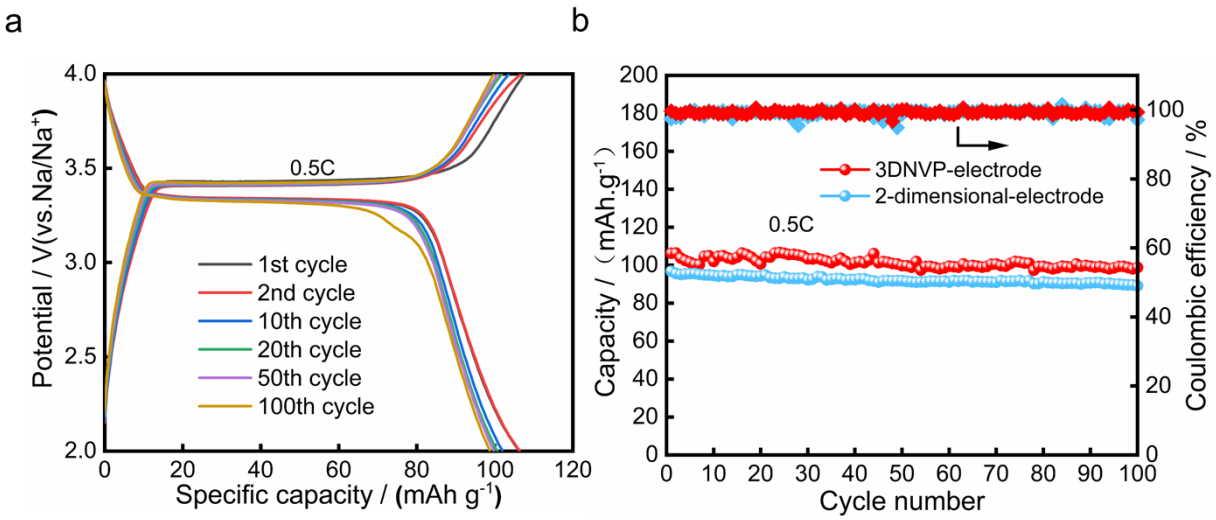

Fig. S8 (a) Galvanostatic charge/discharge profiles at 0.5C under various cycle numbers. (b) Cycling stability of 3D and 2D NVP electrodes at 0.5C.

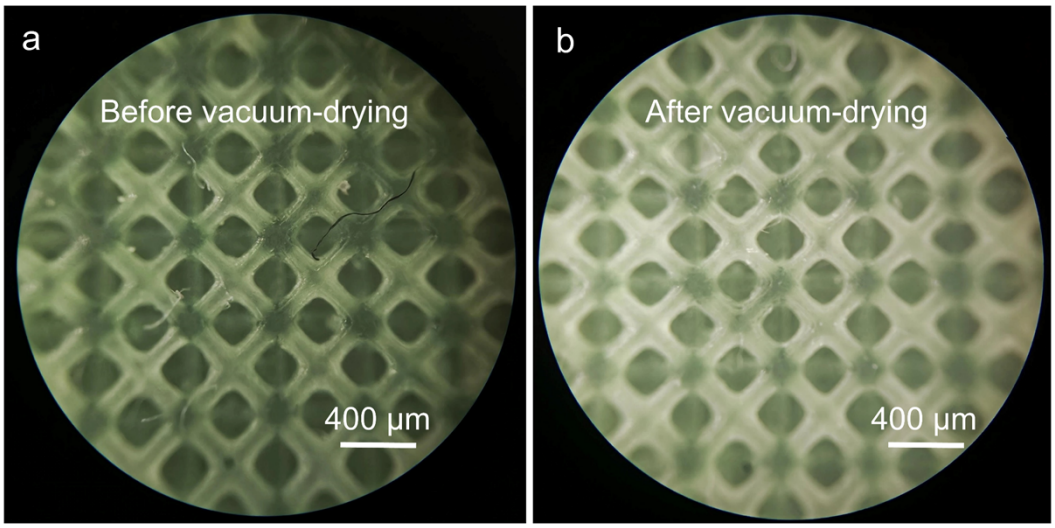

Fig. S9 Optical photographs of the 140 μm beam printed electrode (a) Before vacuum-drying and (b) After vacuum-drying at 80 °C for 12 h.

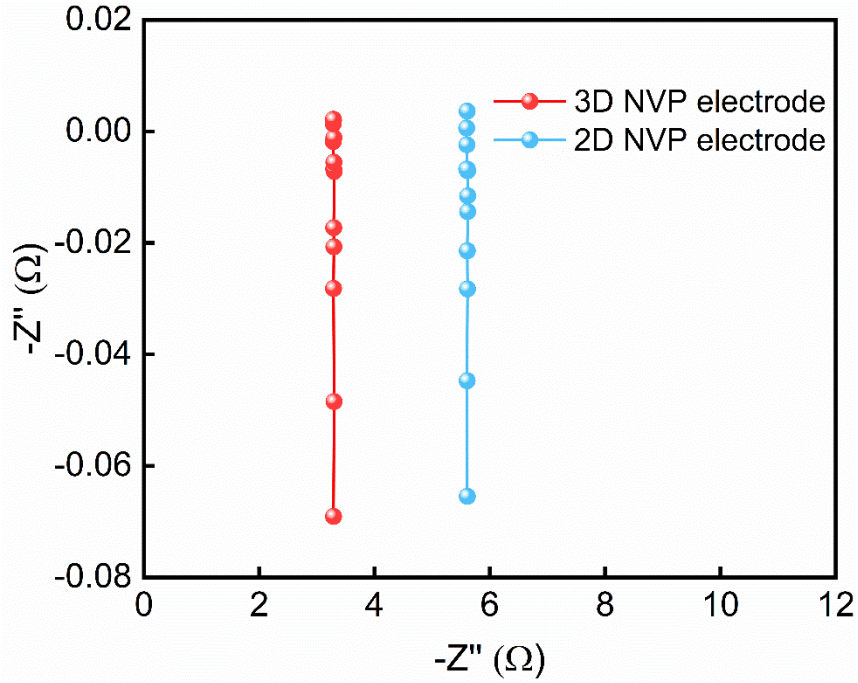

Fig. S10 EIS of 3D NVP electrode and 2D NVP electrode.

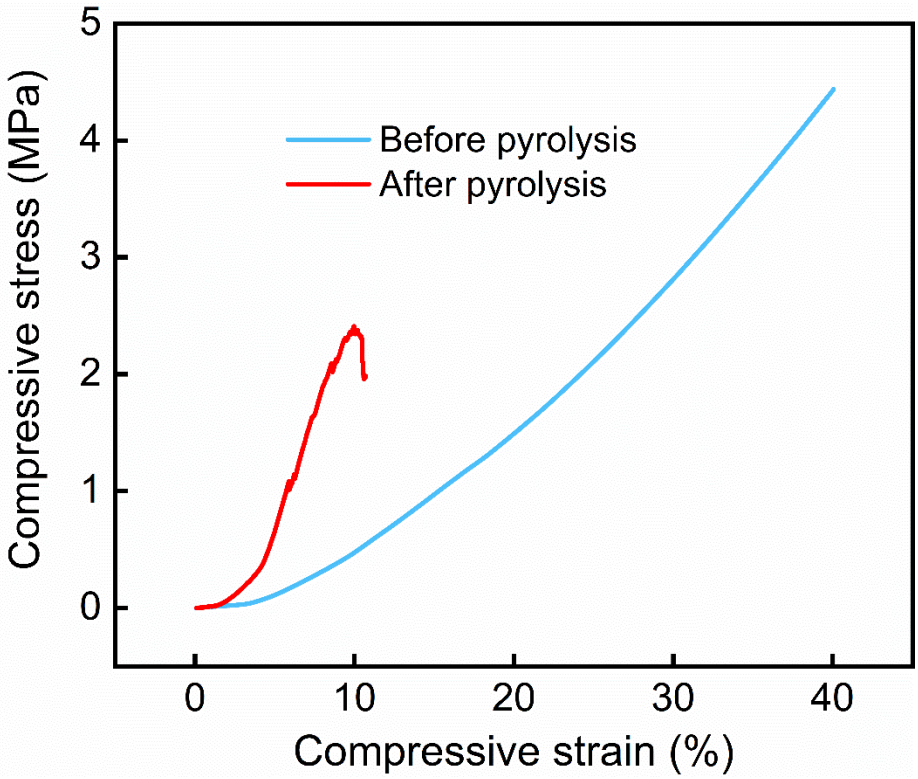

Fig. S11 Compressive stress–strain curves of the 3D printed electrode before and after pyrolysis.

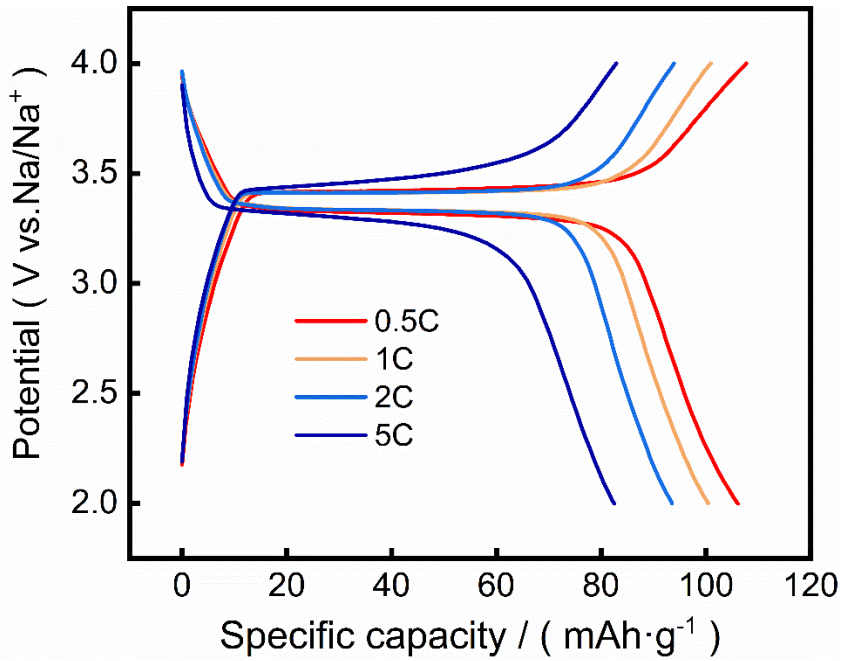

Fig. S12 Galvanostatic charge/discharge profiles of 3D NVP electrode at various current densities.

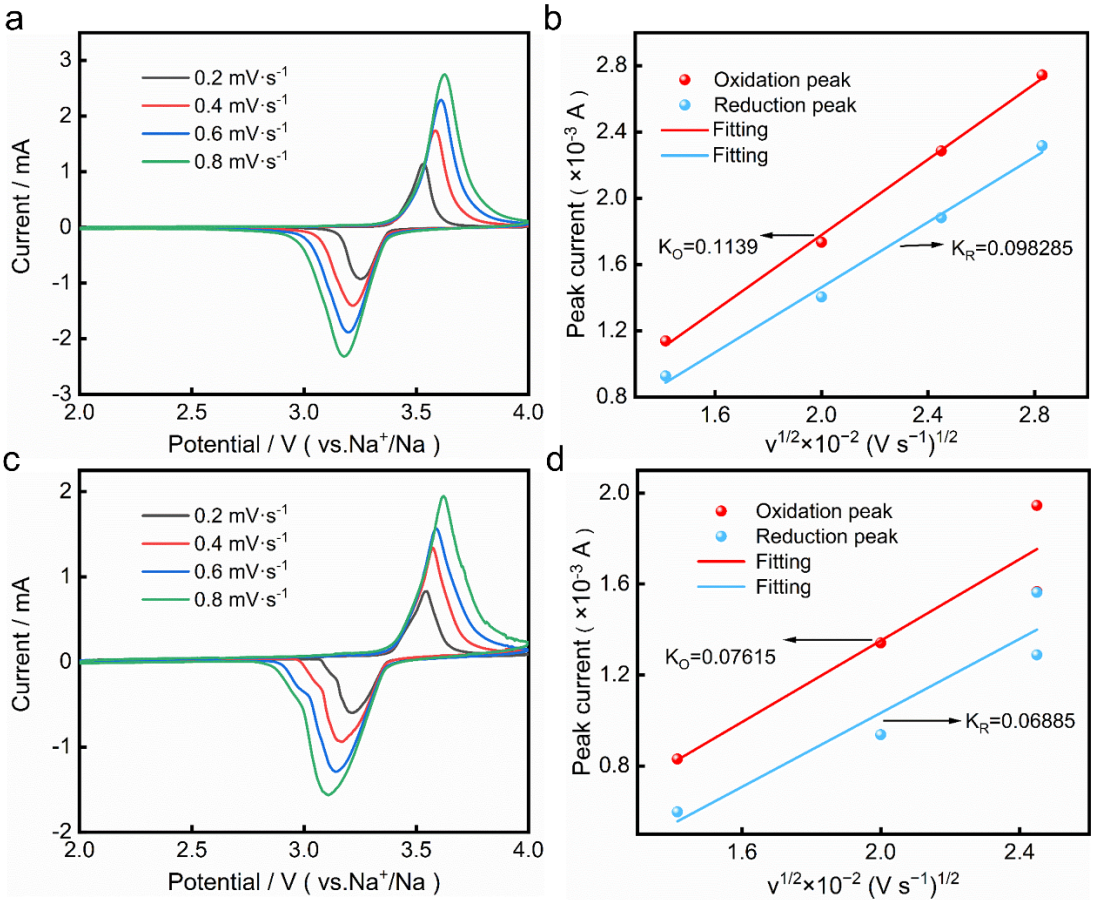

Fig. S13 (a) Cyclic voltammetry curves of the 3D NVP electrode in the second cycle at scan rates of 0.2–0.8 mV s^{-1} within 2.0–4.0 V (vs. Na^+/Na). (b) Corresponding linear fitting plots of peak current versus $v^{1/2}$for the 3D electrode. (c) Cyclic voltammetry curves of the 2D NVP electrode under the same conditions. (d) Corresponding linear fitting plots of peak current versus $v^{1/2}$ for the 2D electrode.

Table S1 Comparison of printing parameters between the resin containing the precursors and the pure resin.

Exposure time	Pure commercial resin	The resin containing the precursors
First layer	35 s	45 s
2-final layer	3 s	6 s

Table S2 Comparison of resistance and electronic conductivity between the 3D NVP electrode and 2D NVP electrode.

Sample	A (cm^2)	L (cm)	Resistance (Ω)	Conductivity (S/cm)
3D NVP electrode	0.0069	0.3	3.285	13.24
2D NVP electrode	0.0060	0.3	5.59	7.78

Table S3 Comparison between DIW and SLA printing.

Comparison aspects	DIW	SLA
Printing accuracy	Moderate to low (typically ≥ 100 μm).[2,3]	High (can reach 10-25 um).
Binder	Required.[4]	Not required.
Structural complexity	Limited. Difficulty in fabricating unsupported.[5]	Excellent. Capable of fabricating sophisticated 3D architectures.[6]
Carbon source	Required.	Precursor-derived (no need to add separately)

Table S4 EIS fitting results of 3D NVP electrode and 2D NVP electrode.

Element	3D NVP electrode	2D NVP electrode
R_s / ($\Omega \cdot cm^{-2}$)	68.16	16.89
R_{ct} / ($\Omega \cdot cm^{-2}$)	259	433.4
CPE1-T / (10^{-6} $\Omega \cdot cm^{-2}$)	1.828	7.564
CPE1-P / ($\Omega \cdot cm^{-2}$)	0.7579	0.6819
W ($\Omega \cdot cm^{-2}$)	0.01126	0.001516

According to the ever report,[7] the equivalent circuit for EIS fitting in SIBs includes the Warburg diffusion impedance (W), charge transfer resistance (R_{ct}), solution resistance (R_s), and constant phase element (CPE). The circuit relationship is that the solution resistance Rs is connected in series with a parallel unit. This parallel unit consists of the constant phase element CPE connected in parallel with another unit, which is the series connection of R_{ct} and the Warburg diffusion impedance W (Fig. 5b). And R_{ct} reflects the rate of electrode interfacial reaction activity and the ease with which charge transfers across the electrode. The fitted R_{ct} of the 3D NVP electrode is 259 Ω, notably lower than the 433.4 Ω obtained for the 2D NVP electrode (Table S2), indicating the positive role of the 3D porous architecture in enhancing overall electrode conductivity.

Table S5 Comparison of performance with other 3D NVP electrode.

Cathode	Capacity	Cycle life	Capacity Retention	Active mass loading	Ref
3D NVP electrode	107 mAh·g^{-1} at 0.5C	500 cycles at 5C	95.9%	21.39 mg·cm^{-2}	**This work**
meso-NVP/C-FD[8]	92 mAh·g^{-1} at 0.1C	300 cycles at 2C	88%	/	8
Nanostructured $Na_3V_2(PO_4)_3$@C[9]	99 mAhg^{-1} at 1C	300 cycles at 2C	80%	/	9
3D CNT decorated $Na_3V_2(PO_4)_3$/C[10]	111.7 mAh g^{-1} at 0.1C	200 cycles at 10C	80.3%	/	10
3DP NVP/MXene cathode[11]	103.8 mAh g^{-1} at 2.5mA·cm^{-2}	450 cycles at 5mA·cm^{-2}	80%	18.4 mg·cm^{-2}	11

Reference

1 S. Clark, T. Zhang, Y. Zhang, J. Yang, L. Li, G. Kang, Guide to assembling a coin cell battery for laboratory testing, *Batteries Supercaps*, 2022, **5**, e202200098.

2 R. Tao, Y. Gu, J.K. Sharma, K. Hong, J. Li, A conformal heat-drying direct ink writing 3D printing for high-performance lithium-ion batteries, *Mater. Today Chem.*, 2023, **32**, 101672.

3 Z. Guo, Z. Chen, Three-dimensional and hierarchically porous bulk battery electrode, *J. Alloys Compd.*, 2016, **685**, 705-709.

4 R. Raj, A.R. Dixit, Direct Ink Writing of Carbon-Doped Polymeric Composite Ink: A Review on Its Requirements and Applications, *3D Print. Addit. Manuf.*, 2023, **10**, 828-854.

5 M. Chen, X. Zhang, W. Yuan, Y. Zhou, Z. Lu, C. Wang, S. Jiang, X. Wu, Y. Ye, Y. Tang, Direct ink writing to create low-tortuosity structured electrodes for advanced sodium-ion batteries, *J. Solid State Electrochem.*, 2025, **29**, 1-11.

6 B. Msallem, J.J. Vavrina, M. Beyer, F.S. Halbeisen, G. Lauer, A. Dragu, F.M. Thieringer, Dimensional Accuracy in 3D Printed Medical Models: A Follow-Up Study on SLA and SLS Technology, *J. Clin. Med.*, 2024, **13**, 5848.

7 D. Ferreira, A. Pinto, R. Silva, C. Costa, P. Marques, Advanced Manufacturing Processes of NASICON-Based All-Solid-State Lithium-Metal Batteries, *Interfaces*, 2025, **17**, 30793-30805.

8 S.M. Chang, C.E. Liu, C.C. Yang, T.F. Hung, Enhanced Performances of Mesoporous $Na_3V_2(PO_4)_3$/C Microparticles: Insights from Morphological and Textural Characteristics, *Electrochim. Acta*, 2025, **514**, 145678.

9 R.S. Kate, R.J. Deokate, S.V. Kadam, M.V. Kulkarni, B.B. Kale, R.S. Kalubarme, Highly Stable and Nanoporous $Na_3V_2(PO_4)_3$@C Cathode Material for Sodium-Ion Batteries Using Thermal Management, *J. Energy Storage*, 2023, **74**, 109245.

10 G. Du, S. Wang, M. Zheng, 3D CNT decorated $Na_3V_2(PO_4)_3$/C microsphere with outstanding sodium storage performance for Na-ion batteries, *Solid State Ionics*, 2018, **317**, 229-233.

11 T. Jiang, Y. Zhang, T.W.L. Du, Two-step electrodeposition synthesis of iron cobalt

selenide and nickel cobalt phosphate heterostructure for hybrid supercapacitors, *J. Colloid Interface Sci.*, 2023, **629**, 1049-1060.